ADVANCED MATERIALS
www.advmat.de

Fast Gas-Adsorption Kinetics in Supraparticle-Based MOF Packings with Hierarchical Porosity

Atsushi Fujiwara, Junwei Wang, Shotaro Hiraide, Alexander Götz, Minoru T. Miyahara, Martin Hartmann, Benjamin Apeleo Zubiri, Erdmann Spiecker, Nicolas Vogel, and Satoshi Watanabe**

Metal–organic frameworks (MOFs) are microporous adsorbents for high-throughput gas separation. Such materials exhibit distinct adsorption characteristics owing to the flexibility of the crystal framework in a nanoparticle, which can be different from its bulk crystal. However, for practical applications, such particles need to be compacted into macroscopic pellets, creating mass-transport limitations. In this work, this problem is addressed by forming materials with structural hierarchy, using a supraparticle-based approach. Spherical supraparticles composed of nanosized MOF particles are fabricated by emulsion templating and they are used as the structural component forming a macroscopic material. Zeolitic imidazolate framework-8 (ZIF-8) particles are used as a model system and the gas-adsorption kinetics of the hierarchical material are compared with conventional pellets without structural hierarchy. It is demonstrated that a pellet packed with supraparticles exhibits a 30 times faster adsorption rate compared to an unstructured ZIF-8 powder pellet. These results underline the importance of controlling structural hierarchy to maximize the performance of existing materials. In the hierarchical MOFs, large macropores between the supraparticles, smaller macropores between individual ZIF-8 primary particles, and micropores inherent to the ZIF-8 framework collude to combine large surface area, defined adsorption sites, and efficient mass transport to enhance performance.

1. Introduction

Metal–organic frameworks (MOFs) form crystalline porous materials from molecular frameworks consisting of metal ions bridged by organic ligands.[1] They exhibit well-defined porosity, large surface area, and tunable pore sizes and structures, owing to the versatile choice of the constituent components.[2] In addition to these features, specific types of MOFs have flexible structural frameworks and exhibit a unique adsorption phenomenon called "gate adsorption". In this case, the guest molecule uptake increases in a stepwise way at a certain threshold pressure (gate pressure) because of the structural transition of the host MOF structure (e.g., from a nonporous closed state to an open porous one).[3] Thanks to these attractive properties, MOFs are promising for various applications such as gas storage,[4] gas separation,[5] sensing,[6] catalysis,[7] and drug delivery.[8]

At the lab-scale, high-throughput separation of CO_2 and CH_4 has been recently demonstrated by utilizing two sequential adsorption columns which are packed with flexible and non-flexible MOFs, respectively.[9] For up-scaling integration into industrial separation processes, packing columns simply with MOF particles results in a large pressure drop, and hence excessive energy consumption. Therefore, shaping micrometer-sized MOF particles into defined macroscopic structural units such as beads and pellets has been studied before and is a key step to enable stable

A. Fujiwara, S. Hiraide, M. T. Miyahara, S. Watanabe
Department of Chemical Engineering
Kyoto University
Katsura, Nishikyo, Kyoto 615–8510, Japan
E-mail: nabe@cheme.kyoto-u.ac.jp

The ORCID identification number(s) for the author(s) of this article can be found under https://doi.org/10.1002/adma.202305980

DOI: 10.1002/adma.202305980

J. Wang, N. Vogel
Institute of Particle Technology
Friedrich-Alexander-Universität Erlangen-Nürnberg
91058 Erlangen, Germany
E-mail: nicolas.vogel@fau.de

A. Götz, B. Apeleo Zubiri, E. Spiecker
Institute of Micro- and Nanostructure Research (IMN) & Center for Nanoanalysis and Electron Microscopy (CENEM)
Friedrich-Alexander-Universität Erlangen-Nürnberg
91058 Erlangen, Germany

M. Hartmann
Erlangen Center for Interface Research and Catalysis
Friedrich-Alexander-Universität Erlangen-Nürnberg
91058 Erlangen, Germany

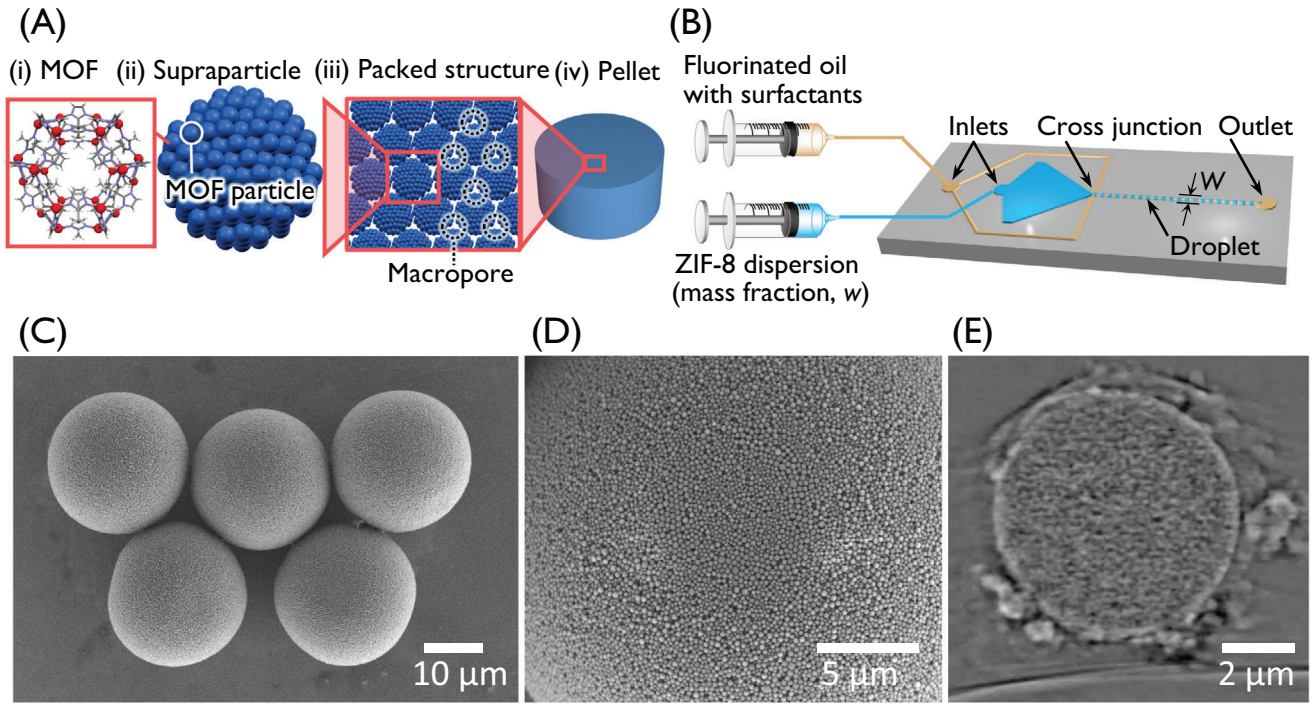

Figure 1. Fabrication of hierarchically structured ZIF-8 materials based on supraparticle building blocks. A) Design strategy: individual ZIF-8 primary particles form supraparticles, which are assembled into macroscopic pellets with structural hierarchy of pores, from micropores to large macropores. B) Schematic illustration of the supraparticle fabrication using a cross-junction microfluidic device. C–E) Structural characterization of ZIF-8 supraparticles fabricated at the mass fraction of ZIF-8 particles $w = 0.02$ and the microchannel width $W = 100$ µm with a 1:1 water–methanol mixture ratio: C) low-magnification and D) high-magnification SEM images of supraparticles and E) cross-sectional slice through a nano X-ray computed tomography (nano-CT) reconstruction of a ZIF-8 supraparticle (please refer to Videos S1 and S2, Supporting Information for animated videos of the tilt series and slices through the 3D reconstruction).

operations.[10] A particularly attractive property of flexible MOFs is their size-dependent adsorption properties.[11] Nanoparticulate MOFs can exhibit different adsorption dynamics compared to their bulk analogs because of different flexibility and/or framework structures.[12] Exploiting this effect in applications requires the creation of macroscopic materials from nanoscale building blocks. In this case, however, even forming beads or pellets fails to provide sufficiently fast mass transport within individual macroscopic units, degrading the overall adsorbent performance. To solve this issue, meso/macropores are incorporated into structural units, as demonstrated by Chen et al. who fabricated hierarchically porous millimeter-sized foams composed of MOF nanoparticles and carboxymethylcelluloses.[13] Developing intraparticle meso/macropores is another approach to improve mass transport. The creation of MOF crystals with ordered macropores formed by using polystyrene beads as templates provided more efficient gas diffusion efficiency compared with that of conventional MOF single crystals.[14] However, these approaches of incorporating meso/macropores decrease the apparent density of MOF structural units and accordingly, the volumetric gas storage capacity. Thus, there is a considerable demand to create macroscopic materials with a well-defined structural hierarchy, which provides both a low mass-transport resistance and a high apparent density.

We address this challenge by creating multilevel hierarchical materials with well-defined internal structure spanning several length scales (**Figure 1**A). In particular, we take advantage of supraparticles (SPs)[15] as intermediate building blocks to create the desired structural hierarchy that bridges the micro- and macropores. Microscopically, our primary MOF particles are in the size range of a few hundred nanometers with sub-nanometer pores (Figure 1A-i). SPs are spherical assemblies with a size in the range up to tens of micrometers, formed by a packing of the primary MOF particles (Figure 1A-ii). The SPs are then packed into a regular macroscopic structure to create the multi-hierarchical material (Figure 1A-iii,iv). Inside each SP, the dense packing of the primary particles minimizes loss in volumetric gas storage, while the interstitial spaces between the primary particles in contact form a first macropore network (Figure 1A-ii). On a larger length scale, the interstitial sites formed between the SPs in contact create a second network of larger macropores. This multi-hierarchical structural design ensures efficient mass transport within the macroscopic material, through two levels of macropore networks into the micropore network of MOF particles (Figure 1A-iii).

SPs can be fabricated by confining a dispersion of primary particles within a droplet. As the solvent evaporates, the volume fraction of the particles continuously increases until they consolidate into a spherical agglomerate when capillary forces force the primary particles into close contact.[15,16] The required droplets can be formed by emulsification, using conventional rotor-stator systems[17] or microfluidic devices[18] to control droplet size and size distribution. Alternatively, droplets can be directly formed on superhydrophobic substrates,[19] albeit with low throughput,

or within spray drying setups, where the consolidation into spherical structures requires careful parameter control.[20] Recent advances in the design of SPs have demonstrated the successful incorporation of mesopores in SPs composed of colloidal silica particles,[21] mesoporous silica particles,[22] and microporous zeolite particles[23] and the formation of consolidated SPs using MOF particles.[24] These studies underline the great potential of creating hierarchical porosity within SPs, yet, to this point, have mainly focused on the structural design of the SPs. Although photonic crystals of MOF particles displayed excellent separation capacity toward organic dye solutions and great potential in the separation field,[25] basic understanding of equilibrium and kinetic adsorption characteristics of SPs is still lacking.

Here, we take the development one step further and explore the functional properties of macroscopic materials formed by such SP building blocks, focusing on gas adsorption as the trademark property of MOF materials. We use zeolitic imidazolate framework-8 (ZIF-8) particles as a model MOF system and fabricate SPs to introduce a second level of hierarchy (Figure 1A). We fundamentally explore how this structural hierarchy affects the adsorption equilibrium and gas-adsorption kinetics, compared to conventional packings of MOF particles without structural hierarchy. We believe that the present study provides an important guideline for the development of pellets with excellent adsorption performance and encourages the development of ordered MOF particle systems as novel porous materials.

2. Results and Discussion

We first synthesized colloidal ZIF-8 particles by mixing aqueous solutions (typically 20 mL each) of zinc nitrate hexahydrate (50 mM) and 2-methylimidazole (3.0 M) in a central-collision type microreactor.[26] The reaction solution was collected in a vial and maintained under a quiescent condition for 1 h. The resultant ZIF-8 particles were washed with methanol by centrifugation at 3500 rpm for 1 h and obtained as a powder by drying overnight under vacuum ($\approx 10^2$ Pa) with a mean particle size of 190 nm (Figure S1, Supporting Information). The XRD pattern (Figure S2, Supporting Information) and the BET surface area of 1508 m^2 g^{-1} confirmed the synthesis of well-ordered ZIF-8 crystals. The synthesized ZIF-8 powder was redispersed in a water–methanol mixture and used as primary building blocks to form SPs. Importantly, this redispersion step was performed in the absence of surfactants to avoid blocking of the ZIF-8 micropores by surfactant adsorption and thus a decrease in adsorption capacity. We found that the addition of methanol increased the dispersibility of ZIF-8 particles (Figure S3, Supporting Information). We formed ZIF-8 dispersion droplets in a microfluidic cross-junction device, using a perfluorinated oil containing a perfluorosurfactant (0.5 wt%) as the continuous oil phase (Figure 1B).[18d,27] We successfully produced spherical SPs with a diameter of 24.9 ± 1.1 μm (Figure 1C) composed of densely packed ZIF-8 primary particles (Figure 1D) by letting the water–methanol mixture of the inner droplets evaporate by diffusion through the oil phase. Nano X-ray computed tomography (nano-CT) analysis revealed that the formed ZIF-8 SPs were fully consolidated into densely packed internal structure, evidenced by a reconstructed cross section through a representative SP (Figure 1E and Video S1, Supporting Information). The ratio of water and methanol in the ZIF-8 dispersion critically affected the SP formation. A 3:1 water–methanol mixture resulted in the formation of buckled SPs with a wide variety in size (Figure S4A, Supporting Information), which we tentatively attribute to premature aggregation of ZIF-8 particles within the droplets as a result of the reduced dispersibility at the increased amount of water (Figure S3, Supporting Information). A 1:3 water–methanol mixture also failed to produce monodispersed SPs, showing broken structures and low yields (Figure S4B, Supporting Information), possibly due to the reduced emulsion stability at higher methanol content. We found that a 1:1 water–methanol mixture used as a dispersion medium allowed both the dispersibility of ZIF-8 particles and the stability of emulsion droplets, thereby yielding monodispersed spherical SPs of ZIF-8 particles (Figure 1C–E).

Using the optimized 1:1 water–methanol mixture of the dispersed phase, we varied the mass fraction of ZIF-8 particles, w, and the microchannel width, W. **Figure 2**A shows the relationship between the SP diameter, D_p, and w for different values of W. Increasing W from 50 to 100 μm under a preset w of 0.05 increased D_p from 20.8 (Figure S5A, Supporting Information) to 46.7 μm (Figure 2B), which is due to a larger droplet size produced in a wider microchannel. For a preset W of 100 μm, increasing w from 0.02 to 0.05 increased D_p from 24.9 (Figure 1C) to 46.7 μm (Figure 2B). A parameter set of high values of both w and W ($w = 0.10$ and $W = 150$ μm) resulted in the largest prepared SPs ($D_p = 79.9$ μm, Figure S5B, Supporting Information). These results indicate that the number of ZIF-8 particles trapped in a single droplet, N_p, directly determines D_p. To confirm this, we calculated N_p and D_p and compared the calculated values with the experimental results. Under simple assumptions that the droplet diameter is identical to W and that ZIF-8 particles are spherical, N_p is given as the following equation.

$$N_p = \left(\frac{W}{d_p}\right)^3 \frac{\rho_{sus}}{\rho_p} w \tag{1}$$

where d_p is the diameter of ZIF-8 particles, and ρ_p and ρ_{sus} are the densities of ZIF-8 (=0.95 g cm^{-3})[28] and a suspension of ZIF-8 particles, respectively. The SP size D_p is then expressed as follows.

$$D_p = d_p \sqrt[3]{\frac{N_p}{\phi}} \tag{2}$$

where ϕ is the volume fraction of ZIF-8 particles in an SP. The calculated results assuming a close-packed structure ($\phi = \pi/(3\sqrt{2})$), which are shown as the dotted lines in Figure 2A, broadly agree with the experimental results, demonstrating that the SPs have a consolidated nature and are packed well within the SPs, corroborating the results of nano-CT (Figure 1E).

Further decrease in w from 0.02 to 0.005 under a fixed W of 100 μm did not produce smaller SPs but resulted in buckled structures as shown in Figure 2C, indicating the existence of experimental constraints in the design of well-defined SPs. We hypothesize that the formation of buckled structures relates to the strong affinity of ZIF-8 particles to the surface of the droplet. We estimate the adsorption energy of a ZIF-8 particle to the interface to the order of $10^2 kT$ (see calculation details and Figure S6, Supporting Information). Figure 2D displays a possible

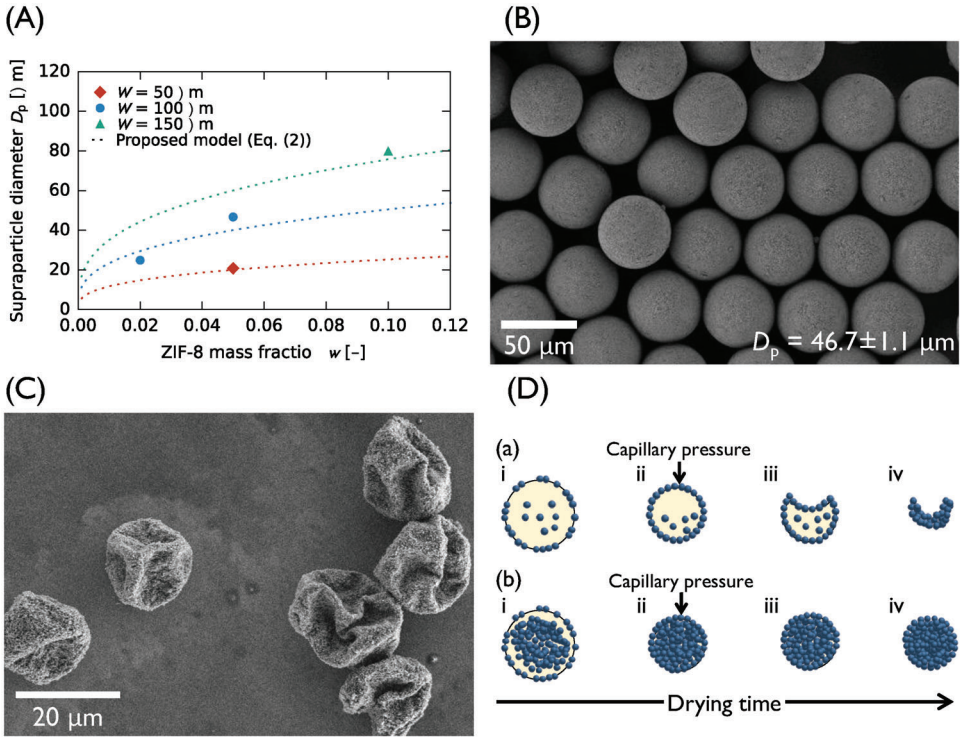

Figure 2. Size and shape variation in spherical supraparticles. A) Effect of w and W on the supraparticle diameter D_p. The dotted lines show the calculated diameters for three different W values based on the proposed model (Equation (2)). B,C) SEM images of supraparticles fabricated at w = 0.05 and W = 100 µm (B) and w = 0.005 and W = 100 µm (C). D) Proposed mechanism for the formation of supraparticles with buckled (a) and spherical (b) structures.

formation pathway leading to buckled structures and spherical SPs, respectively. In the case of low ZIF-8 concentrations under which buckled structures form (Figure 2D-a), most of the ZIF-8 particles in a droplet are trapped at the interface (a-i) because the solvent removal is slow enough for ZIF-8 particles to reach the interface by Brownian diffusion. In fact, a characteristic time for a ZIF-8 particle in a droplet to diffuse across the radius of the droplet is calculated to be 10^3 s, which is shorter by one to two orders of magnitude than the drying time (≈10^4 to 10^5 s) (see calculation details in the Supporting Information). As the dispersion droplet shrinks, the interface is completely covered with ZIF-8 particles to form a particulate shell (a-ii). Once the shell is formed, it subsequently gives in to the stress developed by the capillary pressure[29] and becomes concave toward the center of the droplet (a-iii), resulting in the formation of buckled structures (a-iv). In contrast, with higher numbers of particles within the droplet (Figure 2D-b), even after the attachment of ZIF-8 particles onto the interface, a number of ZIF-8 particles remain dispersed in the droplet (b-i) and form a dense structure upon solvent removal (b-ii). Because of this dense structure of ZIF-8 particles, the concave deformation is hindered (b-iii), resulting in the formation of spherical SPs (b-iv). Based on this assumption, the formation of spherical SPs requires that the surface area that the ZIF-8 particles in a single droplet can potentially cover, $S_{ZIF\text{-}8}$, must be much larger than the surface area of the droplet, S_p. Otherwise, buckled structures would form because all the ZIF-8 particles in a droplet attach to the droplet interface. In fact, as summarized in Table S1, Supporting Information, in our experiments, spherical SPs formed in the case of $S_{ZIF\text{-}8}/S_p$ values larger than 2.5, while buckled structures resulted in a $S_{ZIF\text{-}8}/S_p$ value smaller than 1. Because $S_{ZIF\text{-}8}$ can be calculated by N_p and d_p, the morphology of resultant SPs can be predicted by w, W, and d_p. These investigations suggest that a high w is a key to forming spherical SPs with compact internal structure.

We focused on gas adsorption as the functional property of ZIF-8 MOFs.[2] We first determined the equilibrium N_2 adsorption properties of individual SPs. This investigates whether the densely packed nature within the SP (Figure 1E) hinders transport accessibility to primary particles. To fairly evaluate the performance of the SPs, we used the largest size (79.9 µm in diameter, Figure S5B, Supporting Information) that was available from our fabrication process, because the pressure drop (energy loss) inside SPs is generally proportional to SP size. The largest SP size therefore potentially causes the largest degree of restriction of interior particles. We found that a loose powder of SPs exhibited a N_2 adsorption isotherm identical to that of ZIF-8 powder that went through the same treatment as SPs (i.e., a long-term immersion in a water–methanol mixed solution and subsequent calcination, which was used to remove emulsion-stabilizing fluorosurfactant from the SP powder, as described in the Supporting Information). This confirms that SP formation did not induce any structural limitation to the equilibrium adsorption properties of primary ZIF-8 particles (**Figure 3**A). Note, however, that the treatment leads to a small decrease (≈10%) of overall gas adsorption in both SP and treated ZIF-8 powder as well as a shift in the stepwise uptake[30] at a relative pressure of 2.0 ×

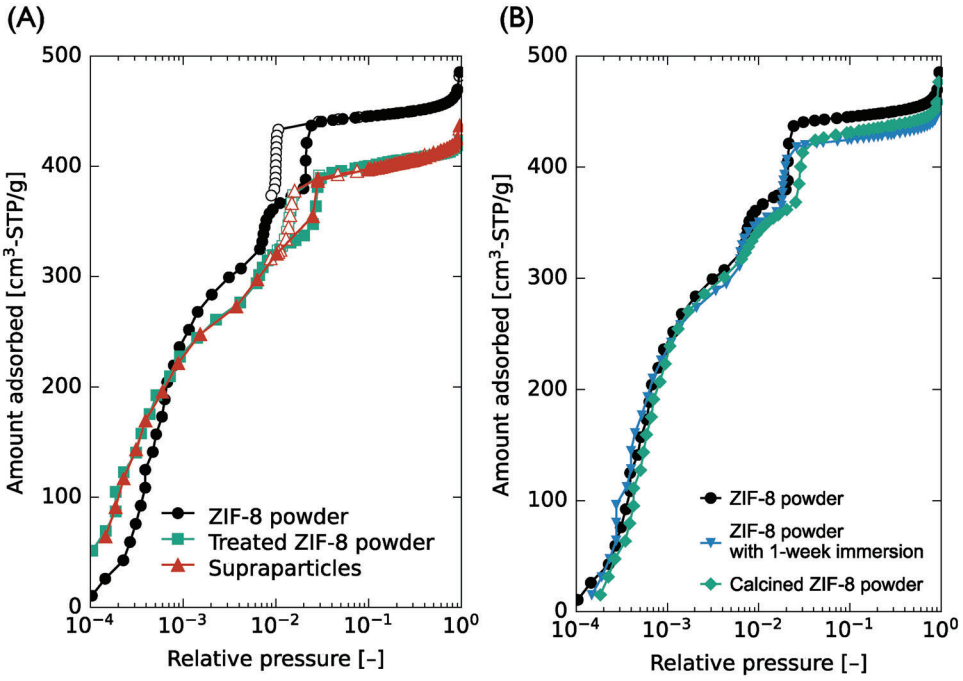

Figure 3. Adsorption properties of ZIF-particles and supraparticles. A) N_2 adsorption/desorption isotherms (77 K) of ZIF-8 powder, treated ZIF-8 powder (solvent immersion and calcination), and the supraparticles composed of ZIF-8 particles. B) N_2 adsorption isotherms (77 K) of ZIF-8 powder, ZIF-8 powder immersed in a water–methanol solution for 1 week, and ZIF-8 powder calcined at 300 °C for 1 h in an air atmosphere.

10^{-2} compared to the initial, untreated ZIF-8 powder (Figure 3A). Through control experiments, we found that the immersion process causes the decrease in the adsorption capacity, possibly due to the partial dissolution of ZIF-8 crystal structures into a water–methanol mixed solution. Meanwhile, the calcination process caused the pressure shift of the stepwise uptake and contributed to the adsorption capacity decrease (Figure 3B). Because we observed that some of the calcined ZIF-8 particles were merged with each other (Figure S7, Supporting Information), the calcination process at 300 °C would have partially fused and damaged the surface structures of ZIF-8 particles.

We then characterized the adsorption properties of macroscopic packings of spherical ZIF-8 SPs and compared them to conventional packings without the intermediate SPs. We hypothesized that the additional level of hierarchy provided by the packing of individual SPs leads to hierarchical porosity within the macroscopic material (Figure 1). In such a hierarchical material, the micropores of the nanoscopic ZIF-8 primary particles are interfaced with an open network of interstitial macropores in the ≈100 nm size range, given by the self-assembled particle structure within the SPs. This first pore network is again interfaced with a larger, interconnected macropore network in the micrometer range, provided by the packing of the SPs. This hierarchical pore network ensures fast and open access to all micropores via the interconnected, double macropore network. We prepared these macroscopic materials by packing the two types of powder (SPs vs primary ZIF-8 particles) into a fluoropolymer tube with a length of ≈1.8 cm (see experimental procedures and Figure S8, Supporting Information). The packing densities of ZIF-8 in tubes calculated from the packed weights were 0.64 and 0.39 g cm^{-3} for ZIF-8 powder and SPs, respectively, while those of the ideal packings with close-packed structures were calculated to be 0.70 and 0.52 g cm^{-3} assuming the ZIF-8 density to be 0.95 g cm^{-3}.[28]

To confirm the existence of this hierarchical pore network, we measured the pore size distributions in the macroscopic packings of ZIF-8 powder and SPs using mercury porosimetry. As shown in **Figure 4**A, the hierarchical material exhibited bimodal macropores with sizes of ≈14 µm and 150 nm, while no pores were detected in the ZIF-8 powder pellet. The larger macropore size in the hierarchical material formed by the second pore network agrees well with the expected size of the interstitial sites between individual SPs given by $(\sqrt{6}-2)D_p/2$, while the smaller macropores evidently corresponded to the first pore network formed by the interstitial sites in the packing of the ZIF-8 primary particles (Figure 4A, black dotted lines). The pore size analysis of the segmented nano-CT reconstruction of a single SP (see Figure S9 and Video S3, Supporting Information) further reveals macropores with sizes around 100 nm formed between the ZIF-8 primary particles. Note that the shift to slightly larger values (154 nm for mercury porosimetry and 100 nm for nano-CT) compared to the theoretical size of a perfectly packed, spherical crystal can be attributed to the packing irregularities within the spherical structure (compare Figure 1D,E and Video S2, Supporting Information) and the size distribution as well as deviations from the spherical shape of the primary particles.

The impact of the hierarchical arrangement on the macroscopic functional properties becomes evident in the kinetics of the gas-adsorption process. Figure 4B compares N_2 adsorption rates at 77 K of the macroscopic packings of ZIF-8 powder and SPs plotted against $(\text{time})^{1/2}$. The adsorption rate of the hierarchical packing formed by the SPs was ≈30 times faster than that of the conventional ZIF-8 packing; the time required to reach

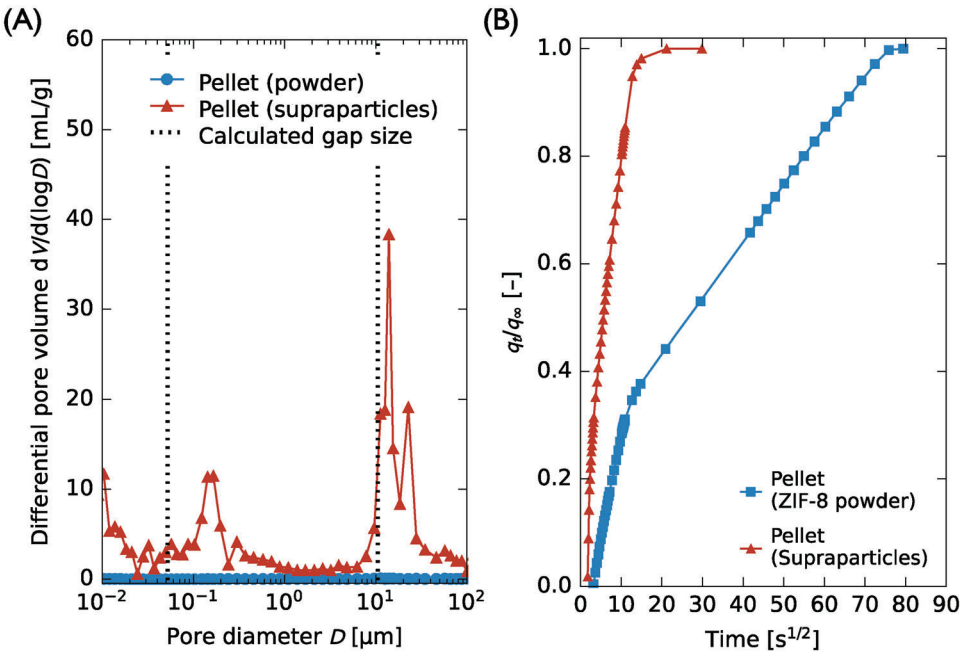

Figure 4. Pore size distribution and kinetic adsorption measurements of pseudo-pellets (Figure S8, Supporting Information), which were fabricated by injecting a methanol suspension of ZIF-8 particles or SPs into a perfluoroalkoxy alkane (PFA) tube and subsequent drying. A) Pore size distributions (from mercury porosimetry) in pellets packed with ZIF-8 powder and the supraparticles. The dotted lines show the theoretical gap sizes between the supraparticles and between primary ZIF-8 particles. B) N_2 adsorption rates of pellets packed with ZIF-8 powder and supraparticles measured with a pressure step of 130 kPa at 77 K, plotted against (time)$^{1/2}$.

95% of the saturation amount ($q_t/q_\infty = 0.95$, where q_t is the adsorption amount at time t and q_∞ is that at equilibrium) was 5000 s for the unstructured ZIF-8 material, while the hierarchical material exhibited a much shorter time of 160 s (see also Figure S10, Supporting Information with linear and logarithmic x-axes). The initial stage of uptake in the macroscopic packing of ZIF-8 powder increased linearly with the square of time, suggesting that the uptake process was controlled by diffusion. More specifically, the uptake rate of N_2 in the macroscopic packing of ZIF-8 powder was much smaller than that in unpacked ZIF-8 powder (see Figure S10, Supporting Information for the comparison of unpacked and packed ZIF-8 powder). For the SPs, by contrast, shaping into the pseudo-pellet did not greatly reduce the uptake rate as in the case of ZIF-8 powder, because of the larger macropores formed between SPs (Figure 4A). The smaller macropores present in individual SPs enhanced the diffusivity in SPs as evident from the adsorption rate in unpacked SPs, which was comparable with that of unpacked powder (see Figure S10, Supporting Information for the comparison of unpacked ZIF-8 powder and SPs). Therefore, the hierarchical pore structure with the much more open macropore space in the pseudo-pellets formed from SPs resulted in a reduced transport resistance. Similar results have been observed for fluid catalytic cracking catalysts[31] and binderless X- and A-zeolites,[32] where additional macropores in beads markedly increase the intraparticle diffusivity of *n*-octane and water, respectively. Details on the factors affecting mass transport in packed beds of porous particles such as length of the packed column, viscosity and density of the fluid, ratio of column diameter to particle diameter, ratio of column length to particle diameter, particle size distribution, particle shape and effect of fluid velocity are given inref. [33]. Their determination is, however, beyond the scope of this paper.

Although the saturated adsorbed amount of the hierarchical material per unit bulk volume was smaller than that of the conventional material due to a lower apparent density, the time to reach a certain adsorption amount, for example, of 150 cm^3-STP cm^{-3}-sample was still approximately ten times faster (Figure S11, Supporting Information). Because our concept is based on a close-packed structure, the packing density of ZIF-8 in the SP pellet (0.39 g cm^{-3}) is higher than those from other shaping techniques (e.g., ≈0.07 g cm^{-3} for hierarchical porous foams[13]), which is a clear advantage of the SP-based hierarchical structure.

3. Conclusions

We have designed a macroscopic MOF material with a hierarchical pore structure consisting of interconnected pore networks at three distinct length scales (>1000; ≈100; ≈1 nm), using a bottom-up, self-assembly process with SPs as intermediate building blocks.

Kinetic adsorption measurements demonstrated a large difference between macroscopic materials with and without structural hierarchy. The adsorption rate of the supraparticle-based material was 30 times faster than that of the unstructured ZIF-8 powder pellet. Mercury porosimetry measurements demonstrated the presence of the anticipated interconnected pore networks with distinct interstitial sites of both SPs and primary particles providing percolation pathways for efficient mass transfer to the actual gas-adsorption sites within the ZIF-8 nanoparticles. This study underlines the importance of a rational structure design

spanning multiple length scales to optimize macroscopic functional properties. Because MOF particles exhibit size-dependent adsorption properties, downsizing to nanoscale can be quite effective to achieve specific adsorption characteristics. In such a case, SPs, with their ability to form secondary structural elements at the microscale, are an emergent, flexible tool to bridge materials design from the nano- to the macroscale.

Supporting Information

Supporting Information is available from the Wiley Online Library or from the author.

Acknowledgements

This work was conducted as a bilateral joint research project funded by the Japan Society for the Promotion of Science (JSPS) and the Deutscher Akademischer Austauschdienst (DAAD) and was also partly supported by the Fund for the Promotion of Joint International Research (Fostering Joint International Research (A), 18KK0411) from JSPS and by the Deutsche Forschungsgemeinschaft (DFG, German Research Foundation)—project-ID 416229255–SFB 1411. Support by CRC 1452 (project ID 431791331) is also acknowledged.

Open access funding enabled and organized by Projekt DEAL.

Conflict of Interest

The authors declare no conflict of interest.

Data Availability Statement

The data that support the findings of this study are available from the corresponding author upon reasonable request.

Keywords

adsorption kinetics, hierarchical porosity, metal–organic frameworks, self-assembly, supraparticles

Received: June 20, 2023
Revised: September 11, 2023
Published online: September 26, 2023

[1] a) S. Kitagawa, R. Kitaura, S.-I. Noro, *Angew. Chem., Int. Ed.* **2004**, *43*, 2334; b) H. Furukawa, K. E. Cordova, M. O'keeffe, O. M. Yaghi, *Science* **2013**, *341*, 1230444.

[2] a) H. Furukawa, N. Ko, Y. B. Go, N. Aratani, S. B. Choi, E. Choi, A. Ö. Yazaydin, R. Q. Snurr, M. O'keeffe, J. Kim, O. M. Yaghi, *Science* **2010**, *329*, 424; b) O. K. Farha, I. Eryazici, N. C. Jeong, B. G. Hauser, C. E. Wilmer, A. A. Sarjeant, R. Q. Snurr, S. T. Nguyen, A. Ö. Yazaydin, J. T. Hupp, *J. Am. Chem. Soc.* **2012**, *134*, 15016.

[3] a) S. Horike, S. Shimomura, S. Kitagawa, *Nat. Chem.* **2009**, *1*, 695; b) J. H. Lee, S. Jeoung, Y. G. Chung, H. R. Moon, *Coord. Chem. Rev.* **2019**, *389*, 161.

[4] L. Mu, B. Liu, H. Liu, Y. Yang, C. Sun, G. Chen, *J. Mater. Chem.* **2012**, *22*, 12246.

[5] C. Zhang, R. P. Lively, K. Zhang, J. R. Johnson, O. Karvan, W. J. Koros, *J. Phys. Chem. Lett.* **2012**, *3*, 2130.

[6] S. Liu, Z. Xiang, Z. Hu, X. Zheng, D. Cao, *J. Mater. Chem.* **2011**, *21*, 6649.

[7] A. Schejn, L. Balan, V. Falk, L. Aranda, G. Medjahdi, R. Schneider, *CrystEngComm* **2014**, *16*, 4493.

[8] C. Y. Sun, C. Qin, X. L. Wang, G. S. Yang, K. Z. Shao, Y. Q. Lan, Z. M. Su, P. Huang, C. G. Wang, E. B. Wang, *Dalton Trans.* **2012**, *41*, 6906.

[9] S. Hiraide, Y. Sakanaka, H. Kajiro, S. Kawaguchi, M. T. Miyahara, H. Tanaka, *Nat. Commun.* **2020**, *11*, 3867.

[10] a) M. Kriesten, J. Vargas Schmitz, J. Siegel, C. E. Smith, M. Kaspereit, M. Hartmann, *Eur. J. Inorg. Chem.* **2019**, *2019*, 4700; b) J. Cousin-Saint-Remi, S. Van Der Perre, T. Segato, M.-P. Delplancke, S. Goderis, H. Terryn, G. Baron, J. Denayer, *ACS Appl. Mater. Interfaces* **2019**, *11*, 13694.

[11] a) S. Tanaka, K. Fujita, Y. Miyake, M. Miyamoto, Y. Hasegawa, T. Makino, S. Van Der Perre, J. Cousin Saint Remi, T. Van Assche, G. V. Baron, J. F. M. Denayer, *J. Phys. Chem. C* **2015**, *119*, 28430; b) D. Tanaka, A. Henke, K. Albrecht, M. Moeller, K. Nakagawa, S. Kitagawa, J. Groll, *Nat. Chem.* **2010**, *2*, 410; c) Y. Sakata, S. Furukawa, M. Kondo, K. Hirai, N. Horike, Y. Takashima, H. Uehara, N. Louvain, M. Meilikhov, T. Tsuruoka, S. Isoda, W. Kosaka, O. Sakata, S. Kitagawa, *Science* **2013**, *339*, 193; d) S. Ohsaki, S. Watanabe, H. Tanaka, M. T. Miyahara, *J. Phys. Chem. C* **2017**, *121*, 20366.

[12] S. Ehrling, H. Miura, I. Senkovska, S. Kaskel, *Trends Chem.* **2021**, *3*, 291.

[13] Y. Chen, X. Huang, S. Zhang, S. Li, S. Cao, X. Pei, J. Zhou, X. Feng, B. Wang, *J. Am. Chem. Soc.* **2016**, *138*, 10810.

[14] K. Shen, L. Zhang, X. Chen, L. Liu, D. Zhang, Y. Han, J. Chen, J. Long, R. Luque, Y. Li, B. Chen, *Science* **2018**, *359*, 206.

[15] a) S. Wintzheimer, T. Granath, M. Oppmann, T. Kister, T. Thai, T. Kraus, N. Vogel, K. Mandel, *ACS Nano* **2018**, *12*, 5093; b) S. Wintzheimer, J. Reichstein, P. Groppe, A. Wolf, B. Fett, H. Zhou, R. Pujales-Paradela, F. Miller, S. Müssig, S. Wenderoth, K. Mandel, *Adv. Funct. Mater.* **2021**, *31*, 2011089.

[16] a) Y. Zhao, L. Shang, Y. Cheng, Z. Gu, *Acc. Chem. Res.* **2014**, *47*, 3632; b) E. S. A. Goerlitzer, R. N. Klupp Taylor, N. Vogel, *Adv. Mater.* **2018**, *30*, 1706654.

[17] A. Plunkett, C. Eldridge, G. A. Schneider, B. Domènech, *J. Phys. Chem. B* **2020**, *124*, 11263.

[18] a) S.-H. Kim, S. Y. Lee, G.-R. Yi, D. J. Pine, S.-M. Yang, *J. Am. Chem. Soc.* **2006**, *128*, 10897; b) T. Brugarolas, F. Tu, D. Lee, *Soft Matter* **2013**, *9*, 9046; c) S.-H. Kim, J.-G. Park, T. M. Choi, V. N. Manoharan, D. A. Weitz, *Nat. Commun.* **2014**, *5*, 3068; d) N. Vogel, S. Utech, G. T. England, T. Shirman, K. R. Phillips, N. Koay, I. B. Burgess, M. Kolle, D. A. Weitz, J. Aizenberg, *Proc. Natl. Acad. Sci. USA* **2015**, *112*, 10845.

[19] a) V. Rastogi, S. Melle, O. G. Calderón, A. A. García, M. Marquez, O. D. Velev, *Adv. Mater.* **2008**, *20*, 4263; b) S. Wooh, H. Huesmann, M. N. Tahir, M. Paven, K. Wichmann, D. Vollmer, W. Tremel, P. Papadopoulos, H.-J. Butt, *Adv. Mater.* **2015**, *27*, 7338.

[20] a) S. Y. Lee, L. Gradon, S. Janeczko, F. Iskandar, K. Okuyama, *ACS Nano* **2010**, *4*, 4717; b) S. Zellmer, G. Garnweitner, T. Breinlinger, T. Kraft, C. Schilde, *ACS Nano* **2015**, *9*, 10749.

[21] A. J. Fijneman, J. Högblom, M. Palmlöf, G. With, M. Persson, H. Friedrich, *Adv. Funct. Mater.* **2020**, *30*, 2002725.

[22] U. Sultan, A. Götz, C. Schlumberger, D. Drobek, G. Bleyer, T. Walter, E. Löwer, U. A. Peuker, M. Thommes, E. Spiecker, B. Apeleo Zubiri, A. Inayat, N. Vogel, *Small* **2023**, *19*, e2300241.

[23] W. Rosas-Arbelaez, A. J. Fijneman, H. Friedrich, A. E. C. Palmqvist, *RSC Adv.* **2020**, *10*, 36459.

[24] J. Wang, Y. Liu, G. Bleyer, E. S. A. Goerlitzer, S. Englisch, T. Przybilla, C. F. Mbah, M. Engel, E. Spiecker, I. Imaz, D. Maspoch, N. Vogel, *Angew. Chem., Int. Ed.* **2022**, *61*, e202117455.

[25] C. Liu, Y.-L. Tong, X.-Q. Yu, H. Shen, Z. Zhu, Q. Li, S. Chen, *ACS Appl. Mater. Interfaces* **2020**, *12*, 2816.

[26] S. Watanabe, S. Ohsaki, T. Hanafusa, K. Takada, H. Tanaka, K. Mae, M. T. Miyahara, *Chem. Eng. J.* **2017**, *313*, 724.

[27] J. Wang, C. F. Mbah, T. Przybilla, B. Apeleo Zubiri, E. Spiecker, M. Engel, N. Vogel, *Nat. Commun.* **2018**, *9*, 5259.
[28] J. C. Tan, T. D. Bennett, A. K. Cheetham, *Proc. Natl. Acad. Sci. USA* **2010**, *107*, 9938.
[29] a) B. Pathak, S. Hatte, S. Basu, *Langmuir* **2017**, *33*, 14123; b) N. Tsapis, E. R. Dufresne, S. S. Sinha, C. S. Riera, J. W. Hutchinson, L. Mahadevan, D. A. Weitz, *Phys. Rev. Lett.* **2005**, *94*, 018302.
[30] a) D. Fairen-Jimenez, S. A. Moggach, M. T. Wharmby, P. A. Wright, S. Parsons, T. Düren, *J. Am. Chem. Soc.* **2011**, *133*, 8900; b) M. E. Casco, Y. Q. Cheng, L. L. Daemen, D. Fairen-Jimenez, E. V. Ramos-Fernández, A. J. Ramirez-Cuesta, J. Silvestre-Albero, *Chem. Commun.* **2016**, *52*, 3639.
[31] P. Kortunov, S. Vasenkov, J. Kärger, M. Fé Elía, M. Perez, M. Stöcker, G. K. Papadopoulos, D. Theodorou, B. Drescher, G. Mcelhiney, B. Bernauer, V. Krystl, M. Kočiřík, A. Zikánová, H. Jirglová, C. Berger, R. Gläser, J. Weitkamp, E. W. Hansen, *Chem. Mater.* **2005**, *17*, 2466.
[32] D. Mehlhorn, R. Valiullin, J. Kärger, K. Schumann, A. Brandt, B. Unger, *Microporous Mesoporous Mater.* **2014**, *188*, 126.
[33] J. M. P. Q. Delgado, *Heat Mass Transfer* **2006**, *42*, 279.